Cement and Concrete Composites 119 (2021) 103993

Contents lists available at ScienceDirect

Cement and Concrete Composites

journal homepage: http://www.elsevier.com/locate/cemconcomp

Spatial distribution of graphite in cement materials used for radioactive waste conditioning: An approach to analysis of neutron tomography data

I. Yu. Zel [a,*], M. Kenessarin [a,b], S.E. Kichanov [a], M. Balasoiu [a,c], D.P. Kozlenko [a], K. Nazarov [a,d], M. Nicu [c], L. Ionascu [c], A.C. Dragolici [c], F. Dragolici [c]

[a] Frank Laboratory of Neutron Physics, Joint Institute for Nuclear Research, 141980, Dubna, Russia
[b] State University "Dubna", 141980, Dubna, Russia
[c] "Horia Hulubei" National Institute of Physics and Engineering, P.O.BOXMG-6, Bucharest-Magurele, Romania
[d] Faculty of Physics and Technical Sciences, L.N. Gumilyov Eurasian National University, 010000, Nur-Sultan, Kazakhstan

ARTICLE INFO

Keywords:
Neutron tomography
Image analysis
Particle size distribution
Elastic moduli
Radioactive waste

ABSTRACT

The spatial arrangement of the graphite inside the cement-based materials has been studied using neutron tomography. The large differences in the neutron attenuation coefficients for the graphite and cement phases and the application of mathematical algorithms for an analysis of the three-dimensional reconstructed data allowed us to obtain the distributions of the average sizes, orientation and shape-related parameters of the graphite particles in studied cement samples. The results of calculations of the elastic properties of the graphite contented cement materials based on the obtained structural features of the morphology of graphite phase are presented.

1. Introduction

The problem of storage, treatment and disposal of solid radioactive wastes from nuclear industries is an acute problem for governments, environmental and scientific communities of the countries that use and develop nuclear energy and technologies [1]. The approaches of the creation of new matrixes for embedding the radioactive waste are subject to the strictest regulatory requirements for the mechanical and chemical properties of the specific matrix material [2]. As a result, the prediction of chemical and mechanical behavior of those materials, its formulation, the preparation and synthesis conditions have a great importance.

The cement materials are a key element in the disposals of radioactive wastes. They have a certain set of properties, and have to satisfy the waste acceptance criteria (WAC) for long-term stability [3]. Now, new methods and formulas of cement materials as conditioning matrices are developed for different types of radioactive wastes in order to improve their chemical and mechanical properties [4,5]. One of the problems of the decrease in the mechanical stability of the cement matrix is the noticeable differences between the mechanical properties of the components [6]. As an example, concretes made of lightweight aggregates are weaker than those made of normal-weight aggregates, mainly due to the lower strength of lightweight aggregates causing more extensive propagation of cracks [7].

In our work, we focus on the non-destructive structural studies of cement materials designed to be used for radioactive reactor graphite waste storage. Reactor graphite itself is a composite material, primary composed of coke filler and binder, and largely embedded with pores and microcracks [8]. The formation and treatment processes of reactor graphite may lead to the development of crystallographic textures of graphite crystals [9], as well as the preferred orientations of cracks [8–10]. The compressive strength of graphite falls in the range of about 30–80 MPa and Young's modulus of graphite is mostly less than 11 GPa [11], while the typical Portland cement has higher values of those parameters [7]. From the view of composite mechanics the cement material containing the reactor graphite may be considered as a three-phase composite material [6,12]: cement paste phase, ITZ and aggregate phase. It is well established [6,7,13] that a large number of factors, from water-cement ratio and volume proportions of all phases to the aggregate size distribution and gradients within the ITZ layer affect the concrete's mechanical properties. The corresponding theoretical models based on elasticity theory and/or mixture rules have been proposed to explain or predict the structurally driven elasticity of cement-based materials, e.g. mixture rule (Voigt-Reuss bounds [7]), Hashin-Shtrikman bounds [12] and methods based on the Eshelby's equivalent medium theory [13–15] accounting for the ITZ influence and

* Corresponding author.
E-mail address: zel@jinr.ru (I.Yu. Zel).

https://doi.org/10.1016/j.cemconcomp.2021.103993
Received 22 October 2020; Received in revised form 15 February 2021; Accepted 22 February 2021
Available online 26 February 2021

size gradation. In particular, in Ref. [15] it was shown, that Young's modulus of concrete increases as the maximum aggregate size increases as well as, when densely graded aggregates are used. Regarding the conditioning of graphite material in cement matrix the complex processes like a fragmentation of graphite particles, an unexpected aggregation of small graphite particles, a non-uniform distribution of graphite material, and the fore-mentioned volume proportions, size gradation and ITZ can provoke an instability of the whole cement-based material.

The stringent requirements for mechanical durability of the cement matrix used for radioactive waste conditioning lead to the necessity of study and validate such materials, development of applied approaches to analyzing the spatial location of graphite fragments inside the cement matrices, obtaining structural data for detecting and predicting of the ways for the mechanical degradation of condition matrices for radioactive graphite wastes. In this context, the possibilities of the neutron tomography method for the non-destructive testing of cement materials are attractive [16,17]. The nature of neutron interactions with matter provides several benefits to the neutron method, including high penetration ability, high sensitivity to a water distribution inside materials, and notable visual contrast between light element containing compounds [17,18]. Regarding the neutron probe for composite materials with graphite inclusions, it should be noted the transparency of the graphite for the thermal neutrons or, in other words, the attenuation coefficient of neutrons for graphite is close to zero [18,19]. As a result, there is a high neutron radiographic contrast between graphite inclusions and the cement matrices.

In order to develop an experimental approach to the non-destructive tests of perspective cement materials for disposal and storage of the radioactive graphite waste, we prepare neutron tomography experiments for several types of cement matrices with some chemical additives used to shrink and reduce the porosity to improve the water tightness. The structural features of graphite inclusions were extracted from the reconstructed three-dimension (3D) model of composite cement materials. Here, we propose a novel approach to the analysis of reconstructed 3D data for estimation of structural and morphological features of the graphite aggregates, as well as for estimation of the effective Young's modulus of composite graphite-contented cement materials.

2. Materials and experimental setup

Several sets of cement composite materials with graphite inclusions were prepared based on Portland cement CEM V [20]. The chemical composition of the composite cement matrix is shown in Table 1.

For this experiment we used samples with the water-cement ratio $w/c = 0.4$. The cement paste was prepared at room temperature. As a result, after the hardening of cement pastes with graphite inclusions, several model objects of composite cement materials were obtained in the form of a parallelepiped with dimensions $10 \times 10 \times 60$ mm^3 (Fig. 1a). To overcome the possibility caused by the shape restrictions, a shapeless piece of cement material sample G3 was prepared. The graphite grains are hidden inside the volume of cement model samples, but both large and small grains of the graphite inclusions on the cutting or breaking slice are visible (Fig. 1b).

All cement samples were obtained using a heavy water D_2O to reduce the effects of incoherent neutron scattering on the hydrogen atoms [18]. To reduce porosity in the cement paste, an appropriate additive Sika [21] was added to samples G2 and G4.

Table 1
Composition of cement pastes used for the preparation of studied cement samples.

Sample label	Composition
G1	CEM V + D_2O + 50 wt% graphite
G2	CEM V + D_2O + 50 wt% graphite +0.5 wt % additive (Sika ®)
G3	CEM V + D_2O + 75 wt% graphite
G4	CEM V + D_2O + 75 wt% graphite + 0.5 wt% additive (Sika ®)

The phase analysis of the cement samples was performed using the DN-6 neutron diffractometer [22] at the IBR-2 high-flux pulsed reactor (Joint Institute for Nuclear Research, Dubna, Russia). The neutron diffraction spectra were obtained at the scattering angle of $2\theta = 90°$. The neutron diffraction patterns were fitted by the profile matching mode using the Fullprof software [23].

The neutron tomography experiments were performed using the neutron radiography and tomography facility [24] at the IBR-2 high-flux pulsed reactor. The neutron radiography data has been obtained by the scintillator-based detector system with a high-resolution CCD camera. The neutron beam dimensions restricted the upper limit of the sample size of 20 cm. 360 neutron radiographic images for the different angular position of the sample relative to the neutron beam direction was used for the tomography reconstruction procedure. The exposure time for one projection was 20 s and resulting measurements lasted for 4 h. The imaging data were corrected by the dark current image and normalized to the image of the incident neutron beam using the ImageJ software [25]. The reconstruction of three-dimensional (3D) data of the studied cement samples was performed by the SYRMEP software [26]. The obtained 3D volume data of voxels are essential for the spatial distribution of the neutron attenuation coefficients of the whole cement sample volume. The dimension of one voxel is $52 \times 52 \times 52$ μm^3. The spatial resolution capabilities of the neutron tomography facility have some restrictions on the minimum size of a resolved item up to 150 μm, or 0.003 mm^3 [24]. The visualization and analysis of reconstructed 3D models were performed using VGStudio MAX software (Volume Graphics, Heidelberg, Germany).

3. Results and discussion

3.1. Neutron diffraction

The neutron diffraction method was used for the primary phase analysis of composite cement materials. All studied cement samples are characterized by similar neutron diffraction patterns, which are presented in Fig. 2.

The most intense diffraction peaks correspond to the graphite phase with the crystal structure described by the $P6_3/mmc$ space group with unit cell parameters $a = 2.438(5)$ Å and $c = 6.674(4)$ Å [27]. Other diffraction peaks corresponded to ettringite and calcium hydroxide (portlandite) crystalline phases [28]. There are no unexpected crystal phases as a possible result of the chemical interaction between graphite and the cement matrix, or the fraction of these phases is insignificant.

3.2. Neutron tomography

The spatial distribution of the graphite component in the volumes of the studied cements was measured using the neutron tomography method. A large difference in the neutron attenuation coefficients of the cement and graphite phases causes a high neutron radiographic contrast in the tomographic experiments. The reconstructed 3D models of the studied cement samples are presented in Fig. 3. As expected, the graphite inclusions with the complex shapes and aggregations are visible against the cement matrix in the neutron tomography experiments. There were large graphite aggregates with lengths up to a centimeter found in one of the samples G2 (Fig. 3). It should be noted that, in contrast to the previous studies of the cement matrices with an aluminium powder [29], for all studied cement samples, the uniform distribution of water was observed. Several neutron-transparent areas are assigned to air-filled pores. Small roundish pores were detected in G1 and G3 samples. The irregularities of samples surface caused by the formation of cavities at the boundaries of the container, particularly due to cement shrinkage and mixing procedures, are also visible in the reconstructed data (Fig. 3).

The processing of 3D reconstructed data was performed in three

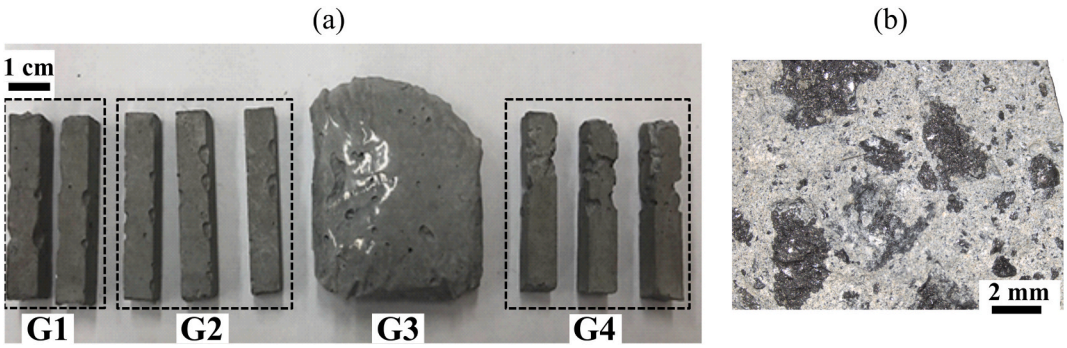

Fig. 1. a) Photography of the studied samples of composite cement with graphite. b) The microscope image of the section of G4 sample after mechanical slicing. The bright regions correspond to the cement material, the black areas are the graphite inclusions.

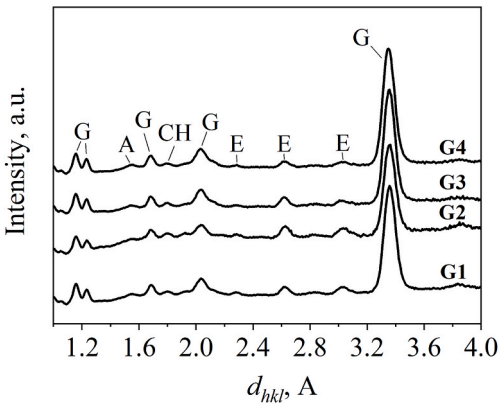

Fig. 2. Neutron diffraction patterns of the composite cement samples. Major phases are labeled as G – graphite, E – ettringite, CH – portlandite, A – alite.

steps (e.g. Ref. [30]): segmentation of graphite phase, separation of graphite particles and its labeling. On the segmentation step, we determined the threshold levels, corresponding to pores with about zero neutron attenuation coefficient and graphite phase with a higher neutron attenuation (e.g. Refs. [19,31]). The obtained 3D binary arrays of graphite phase were further subjected to the separation process, including widely used watershed algorithm. After the separation procedure, the total 3D reconstructed volume of the cement materials was divided into two volumes corresponding to the graphite and cement components. The separated 3D volume of the graphite inclusions in the cement materials is shown in Fig. 3. As an example of the calculations, the reconstructed volumes of the composite cement volume of the sample G3 forms by 50529315 voxels, but the graphite component consists of 9701629 voxels, which corresponds to the estimated volume fraction of graphite in cement sample of 19.2%. The values of 11.2%, 12.1%, and 18.7% were obtained for sample G1, G2, and G4, respectively. This result agrees with the weight fractions of graphite (Table 1) used in the synthesis of studied cement materials.

The calculations were performed to obtain important morphological aspects of graphite grains and aggregates. Commonly used morphological measures in particle analysis comprise different quantities for size determination, such as equivalent diameter, Feret diameter, sieve filter; and shape parameters, such as sphericity, elongation (or aspect ratio), convexity, fractality, etc. [32,33]. However, it should be noted, that physical properties of heterogeneous materials can be successfully described through the homogenization models in which the shape of inhomogeneity inclusions are approximated by the spheroids or

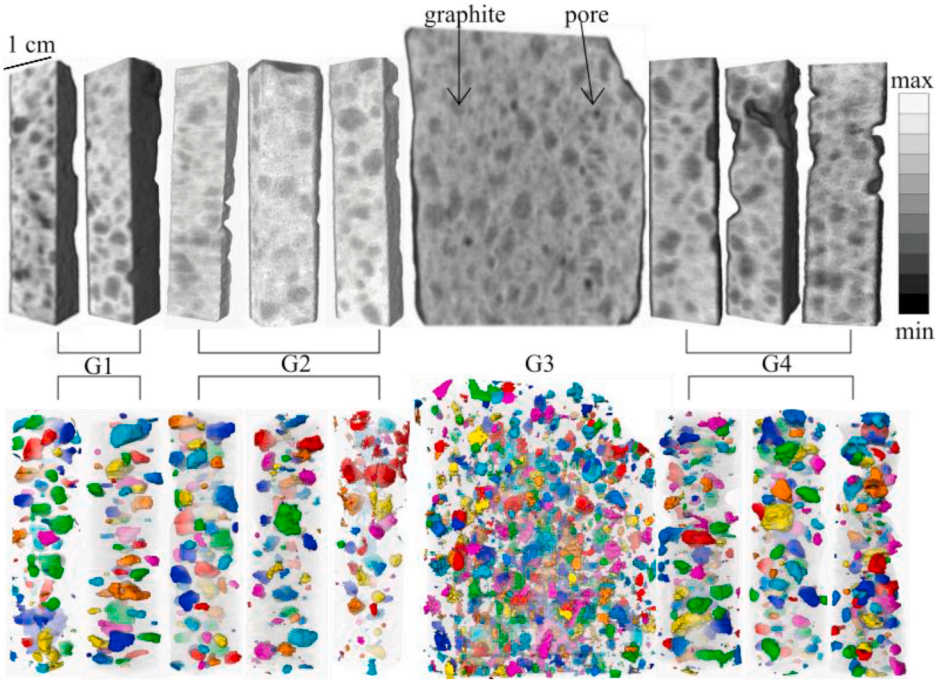

Fig. 3. The upper row: the virtual 3D model of composite cement samples G1, G2, G3, and G4 after tomographic reconstruction. The dark regions correspond to low neutron attenuation in the graphite and pore phases. The gray areas are high neutron attenuation regions of cement materials as also indicated by the colorbar. Examples of pore and graphite inclusion are labeled. In bottom: the separated 3D virtual regions correspond to the graphite grains and aggregates inside the cement samples. The coloring of graphite phase is applied for image perception improving.

ellipsoids [34]. Following this homogenization approach, we analyzed the graphite phase through the ideal shape approximations.

Spherical approximation of graphite grains and aggregates was performed through the determination of their equivalent diameters (D_{eq}) – scalar quantity of particle size, describing the primitive approximation of particle shape by a sphere of the same volume. The anisotropic character of the particle shape was considered in the ellipsoidal approximation, utilizing the concept of an equivalent ellipsoidal body having the same inertia moment as the particle has. It is Legendre ellipsoid [35]. An example of the segmented 3D model of one of the samples G2, as well as the model of Legendre ellipsoid based on separated tomography data, are shown in Fig. 4.

However, such representation requires the determination of local coordinate system of an ellipsoid with respect to the reference axes corresponding to the laboratory coordinate system (Fig. 4). Local coordinate system was determined through three orthonormal principal axes of the inertia moment of the particle (I_{max}, I_{int}, I_{min}). Legendre ellipsoid of the selected graphite particle as shown in Fig. 4 was plotted in local coordinate system according to the equation, adopted from Ref. [35]:

$$\frac{X^2}{\sum x^2}+\frac{Y^2}{\sum y^2}+\frac{Z^2}{\sum z^2}=\frac{5}{N} \quad (1)$$

where X, Y, Z, and x, y, z are the orthogonal coordinates of the Legendre ellipsoid and corresponded voxels of the graphite grain or aggregate, respectively; N – total number of graphite voxels. The semiaxes of ellipsoid (a, b, c) can be determined directly from equation (1) or through the principal values (I_{max}, I_{int}, I_{min}), using well-known expressions [36]. We used the convention for particle coordinate system in which the axis of I_{min} – X-axis, axis of I_{int} – Y-axis, axis of I_{max} – Z-axis, thus the relation $a \geq b \geq c$ is satisfied. Besides, we introduced the shape parameter er, which defines the ratio of axes a/c, as a deviation of ellipsoid from an ideal sphere.

The calculations performed within the described approximations provide the assessment of particle size by equivalent diameter D_{eq}, by maximum and minimum semi-axes a, c and elongation of particle shape by parameter er of the separated graphite inclusions (Fig. 5). We should note that the largest graphite aggregations found in the G2 sample were excluded from the calculations, because they comprise several graphite particles and such aggregate's morphology parameters don't represent the statistics of all graphite phase morphology.

The distribution of the equivalent diameter (Fig. 5a) of graphite grains in studied samples of composite cement materials does not differ much from sample to sample. The distribution of D_{eq} for all samples has a unimodal form with a mean value of 2.64 mm and a standard deviation of 1.02 mm. There is a small shift of the distribution of the diameters to the smaller dimensions range of 1 mm for the G3 sample. However, it seems to us that this shift is due to the larger number of graphite grains in the larger cement volume, and, as a result, reflecting the better sampling for the statistics. The samples G3 and G4 have the average sizes of graphite grains that are somewhat larger than for other samples what may be explained by the presence of aggregated grains as well as by the complexity in separation of the grains in a media with a higher content of graphite.

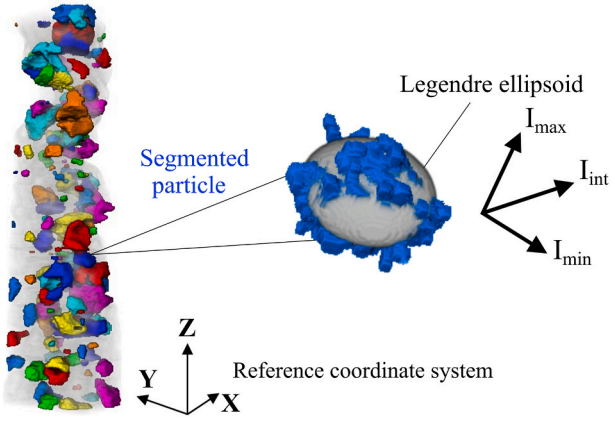

Figure 4. 3D model of G2 sample and virtually extracted graphite particle with Legendre ellipsoid approximation. The principal inertia axes of ellipsoid are shown. The Cartesian coordinates associated with the sample orientation in the tomography experiments are presented as reference coordinate system.

The shape parameter er shows almost no deviations from the average value of all samples (Fig. 5b), which is determined to be about of 2.2 a.u. The distribution of er for the sample G2 has a noticeable peak at ~3.2 a.u., which is the result of weak aggregation of graphite grains leading to the more elongated shapes. The presence of non-spherical graphite grains and the tendency of their shapes to the larger elongation of the corresponding Legendre ellipsoids with increasing size of the graphite grains in studied cement materials are observed through the correlation plot shown in Fig. 5c. Although the ratio of principal ellipsoid axes a/c holds almost constant value of about 2.2 a.u. regardless of the average size of the grains, it is seen (Fig. 5c) that the correlation of minimal c and maximal a axes has a slightly nonlinear trend, which can be related to the specifics of the milling process as well as an aggregation of graphite grains.

The obtained results provide the demonstrative view of the capabilities of the neutron tomography method for the non-destructive structural diagnostics of cement materials with solid graphite inclusions. The approach to the analysis of structural data provides both spatial distribution and morphological parameters of unknown shapeless fragments of radioactive graphite distributed inside the cement volume. However, it should be also noted that it is possible to analyze the orientation of graphite grains in the composite cement materials. The orientation distribution is the basic concept of texture analysis [37], which provides the relation of structural ordering to the anisotropy of physical, including mechanical, properties of composite crystalline materials. In context of composite cement materials, even for space-disordered aggregates there might be an ordering in their shape orientations, produced by technological or other processes.

To reveal the possible orientation ordering of the shapes of graphite grains and aggregates we analyzed the orientations of their local coordinate systems defined by the principal axes of inertia moment of Legendre ellipsoids in relation to the fixed laboratory axes (X, Y, Z). It should be noted that this representation is independent on the shape or volume of the sample. We selected the rotation axis of the sample in the neutron tomographic experiment as the Z-axis (see also Fig. 4). Although the performed analysis has not evidenced strong preferred orientation of graphite particles, we found the notable differences in the orientations of I_{max} axes (or c-axes) among cement samples (Fig. 6). The axis distributions obtained for cement samples G1 and G2 have predominantly random character with some concentration of I_{max} axes subparallel to the laboratory Z-axis, in the center of the projection figure (Fig. 6). However, the graphite grains inside the cement samples G3 and G4 show more dense distribution around the Z-axis than for other samples. This indicates the formation of weak preferred orientation of smallest semi-axis of the approximated Legendre ellipsoids around the laboratory Z-axis. We supposed that this may be the result of the higher concentration of graphite material in the cement matrix, which leads to a denser packing of elongated grains relatively to the larger axis of the sample under container shape restrictions during synthesis process of the cement materials.

As a final step, we want to demonstrate the possibility of calculating the mechanical properties, like the effective Young's modulus E of the studied composite materials using structural parameters obtained from the neutron tomography. Here, we performed the calculations based on two different schemes: the four-phase sphere model [15], that takes into account the influence of graphite grain sizes and an interfacial transition zone (ITZ); and GMS method [10] (GEO-MIX-SELF) which allows one to

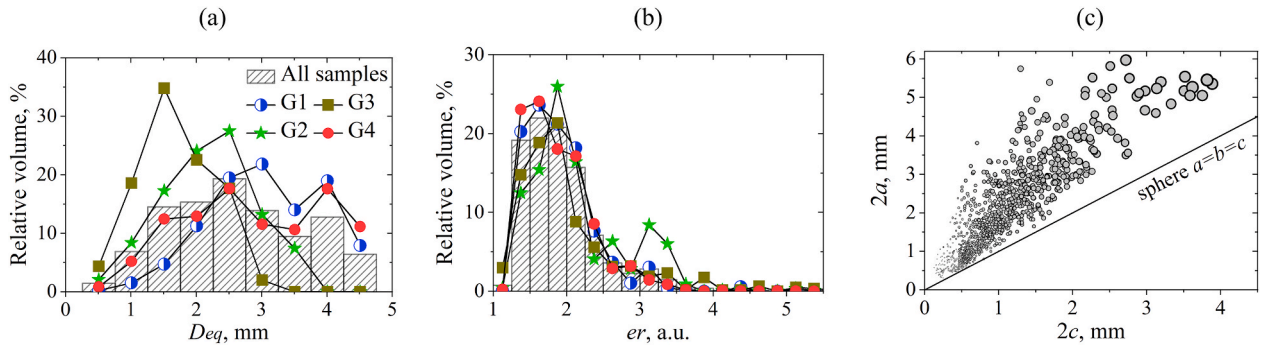

Fig. 5. The distributions of the equivalent diameter D_{eq} (a), the shape parameter er (b) and the relation between ellipsoid semi-axes a and c (c); the diameter of symbols is proportional to the equivalent diameter D_{eq}.

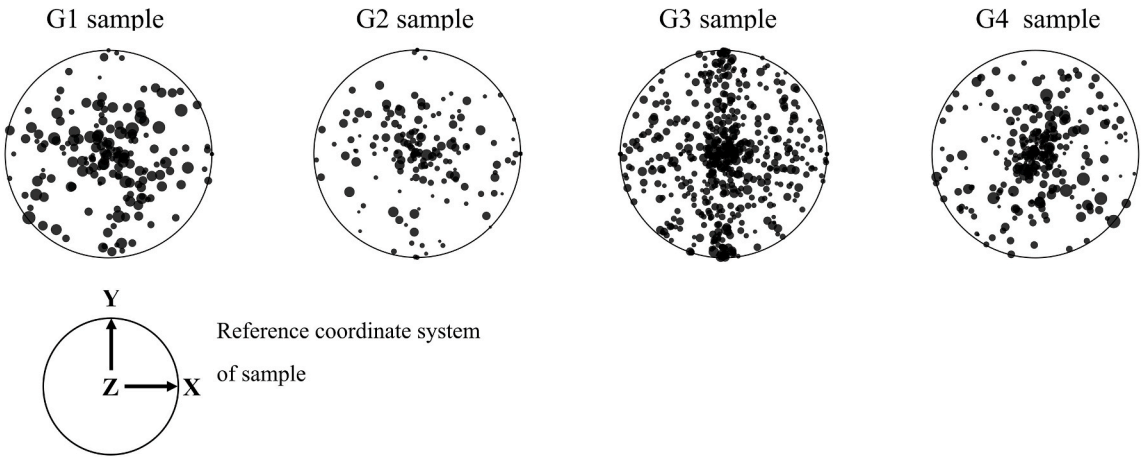

Fig. 6. Stereographic projection of the distributions of the maximum inertia moment I_{max} axes of graphite grains and aggregates. The size of the symbol is proportional to the equivalent diameter D_{eq} of each graphite grain. The orientation of the laboratory coordinate system is shown for the reference.

account the effect of elongated shapes of grains, but ignoring the presence of ITZ layer.

Within the four-phase model the cement material is built up from basic elements of a spherical shape, consisted of aggregate core, ITZ layer and outer layer of cement paste [15]. This model requires a detailed gradation data of grains sizes. The equivalent diameter of graphite inclusions was obtained directly from neutron tomography data (Fig. 5a), and we used those structural data for the calculations. The experimentally obtained values of the average volume fraction of the graphite phase of approximately 12% in cement samples G1 and G2 and 19% for cement samples G3 and G4 were used in the calculations. This pair of values correspond to the two formal cases with low and high graphite content. The volume fraction of the interfacial transition zone (ITZ) around graphite grains was estimated as $6h\frac{1}{D_{eq}}$ times less than volume fraction of the graphite phase, where $h = 0.05$ mm stands for the ITZ thickness [6]. The Young's modulus E for graphite is taken as 6 GPa corresponding to the reactor graphite of GR grade (Table 1in Ref. [11]), while for ITZ it was less by a factor of 0.4 [15]. Poisson ratios were estimated as 0.1 for the graphite, 0.3 for ITZ, and 0.25 for the cement material [15].

In GMS method the composite, particularly cement composite, is presented by ellipsoidal inclusions of different sort (elastic moduli, aspect ratio – (1, b/a, c/a), orientation), embedded to the homogeneous matrix [10]. In our calculations the role of homogeneous matrix was given to the pure cement material (same as for four-phase model). Graphite inclusions in form of ellipsoids were supposed to be randomly oriented with the averaged aspect ratio of (1, 0.72, 0.51) as obtained from statistical analysis of Legendre ellipsoid shapes and to have identical elastic constants as for polycrystalline graphite (same as for four-phase model). In this GMS model we used only one case of graphite content with value of 12% in order to evaluate only the effect of elongate graphite grain shapes.

The results of the calculations for both models are presented in Fig. 7. It can be seen that an increase in the Young's modulus of the concrete is obviously followed the hardening of the cement matrix. The influence of graphite additives becomes noticeable, starting from values of 15–20 GPa of cement Young modulus. At these points the models become to deviate from each other showing the difference in the effects of grain shape, ITZ and graphite volume fraction. At higher values of 40–45 GPa of the Young's modulus of the cement material, the differences in comparison with the concrete increased up to ~2 times. When the volume fraction of graphite increases, the mechanical properties of the cement system also degrade as it was shown within the four-phase model (Fig. 7). It should be noted the predictions for Young's modulus from GMS model are systematically higher than for four-phase model due to the absence of ITZ layer in the model, acting in some way as additional weak phase. Therefore, the effect of elongated shape of graphite aggregates is smaller, than the influence of ITZ. However, we suppose that the combination of ellipsoidal shape with ITZ will enhance the influence of graphite aggregates to the degradation of bulk mechanical properties of cement composite. In this context, attention should be also paid to the nonuniform distribution of graphite grains in cement matrices, including the effects of the elongated particles, which provokes the existing of the preferred orientations and directions, and, as a result, the formation of undesirable anisotropy of mechanical properties of composite cement systems.

In our work, we tried to show the possibilities of the neutron tomography method in the non-destructive testing of the composite

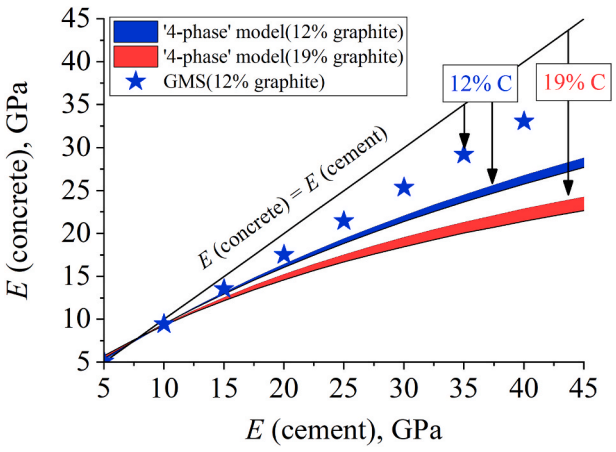

Fig. 7. Calculated Youngs modulus of studied composite cement materials with graphite inclusions in comparison to the cement matrix properties. The shadowed patterns represent the regions within the isostrain-isostress bounds calculated for the four-phase models [28] with 12% and 19% volume fractions of graphite, and the stars represent the calculations within the GMS model [29] for 12% volume fraction of graphite. The structural data for the graphite inclusions used in the presented calculations was obtained from neutron tomography data.

cement materials with graphite inclusions. The neutron radiographic contrast formation for such composite materials, the approaches to the analysis of three-dimensional data, and calculations based on the structural results of the elastic properties of these cement materials can recommend the neutron tomography method as one of the experimental methods for structural diagnosing the mechanical properties of cement materials for the storage and dispose of the radioactive solid graphite.

4. Conclusions

In our work, the model composite cement materials with graphite inclusions were studied by neutron tomography method. The high neutron radiographic contrast between graphite inclusions and the cement material provides opportunities to distinguish grains and aggregates of graphite inclusions from the total volume of composite cement materials in 3D virtual model, determine their spatial locations in the cement materials, and obtain structural and morphological parameters of the graphite inclusions. We used a sphere and an ellipsoid approximations for the shape of graphite grains in the analysis of reconstructed 3D data, and obtained the distributions for the average grain size and the histograms for the grain shape elongation. The estimated preferred orientation of the graphite grain shapes in cement materials was analyzed. The structural features of the graphite inclusions obtained from 3D neutron tomography data were used to calculate the mechanical properties of composite cement materials in the framework of several models that take into account the shape and size of the graphite aggregates. The calculation results have shown the effect of graphite volume content, interfacial transition zone and non-spherical grain shape in weakening of concrete elastic properties. We believe that the presented capabilities of the neutron tomography method and the corresponding algorithms for analyzing the related 3D data could be used in the development of non-destructive experimental approaches for structural diagnostics of composite cement materials for storage and disposal of radioactive graphite solid waste.

Declaration of competing interest

There is no conflict of interest.

Acknowledgements

The work was supported by the Plenipotentiary of Romania to JINR, Dubna, Program “The cementitious materials used for encapsulation of radioactive wastes: neutron scattering studies”.

References

[1] M.I. Ojovan, A.J. Wickham, Treatment of irradiated graphite to meet acceptance criteria for waste disposal: problem and Solutions, Mater. Res. Soc. Symp. Proc. 1665 (2014) 3–12.
[2] Characterization, Treatment and Conditioning of Radioactive Graphite from Decommissioning of Nuclear Reactors, IAEA-TECDOC-1521, IAEA, Vienna, 2006.
[3] P. Faucon, F. Adenot, J.F. Jacquinot, J.C. Petit, R. Cabrillac, M. Jorda, Long-term behaviour of cement pastes used for nuclear waste disposal: review of physico-chemical mechanisms of water degradation, Cement Concr. Res. 28 (1998) 847–857.
[4] C. Poinssot, S. Gin, Long-term behaviour of cement pastes used for nuclear waste disposal: review of physico-chemical mechanisms of water degradation, J. Nucl. Mater. 420 (2012) 182–192.
[5] B. Ilić, V. Radonjanin, M. Malešev, M. Zdujić, A. Mitrović, Study on the addition effect of metakaolin and mechanically activated kaolin on cement strength and microstructure under different curing conditions, Construct. Build. Mater. 133 (2017) 243–252.
[6] P.K. Mehta, P.J.M. Monteiro, Concrete: Microstructure, Properties, and Materials, third ed., McGraw-Hill, 2006.
[7] I. Soroka, Portland Cement Paste and Concrete, McMillan, London, 1979.
[8] J. Kane, C. Karthik, D.P. Butt, W.E. Windes, R. Ubic, Microstructural characterization and pore structure analysis of nuclear graphite, J. Nucl. Mater. 415 (2) (2011) 189–197, https://doi.org/10.1016/j.jnucmat.2011.05.053.
[9] T. Lokajicek, P. Lukas, A.N. Nikitin, I.V. Papushkin, V.V. Sumin, R.N. Vasin, The determination of the elastic properties of an anisotropic polycrystalline graphite using neutron diffraction and ultrasonic measurements, Carbon 49 (4) (2011) 1374–1384, https://doi.org/10.1016/j.carbon.2010.12.003.
[10] S. Matthies, GEO-MIX-SELF calculations of the elastic properties of a textured graphite sample at different hydrostatic pressures, J. Appl. Crystallogr. 45 (2012) 1–16.
[11] Yu Virgil’ev, I.P. Kalyagina, Reactor graphite, Inorg. Mater. 39 (2003) 46–58.
[12] A.U. Nilsen, P.J.M. Monteiro, Concrete: a three phase material, Cement Concr. Res. 23 (1993) 147–151.
[13] J.C. Nadeau, A multiscale model for effective moduli of concrete incorporating ITZ water–cement ratio gradients, aggregate size distributions, and entrapped voids, Cement Concr. Res. 33 (1) (2003) 103–113, https://doi.org/10.1016/s0008-8846(02)00931-6.
[14] C.C. Yang, Effect of the transition zone on the elastic moduli of mortar, Cement Concr. Res. 28 (1998) 727–736, https://doi.org/10.1016/s0008-8846(98)00035-0.
[15] G. Li, Y. Zhao, S. Pang, Y. Li, Effective Young’s modulus estimation of concrete, Cement Concr. Res. 29 (1999) 1455–1462.
[16] Z. Drace, I. Mele, M.I. Ojovan, R.O. Abdel Rahman, An overview of research activities on cementitious materials for radioactive waste management, Mater. Res. Soc. Symp. Proc. 1475 (2012) 253–264, https://doi.org/10.1557/opl.2012.584.
[17] P. Zhang, F.H. Wittmann, P. Lura, H.S. Müller, S. Han, T. Zhao, Application of neutron imaging to investigate fundamental aspects of durability of cement-based materials: a review, Cement Concr. Res. 108 (2018) 152–166, https://doi.org/10.1016/j.cemconres.2018.03.003.
[18] V. F Sears, Neutron scattering lengths and cross sections, Neutron News 3 (1992) 26–37.
[19] M. Adib, Y. Abbas, N. Habib, M. Wahba, M. Fathaallah, Attenuation of thermal neutron through Graphite, Conference on Nuclear and Particle Physics 4 (2003) 257–269.
[20] G. Bye, Portland Cement, ICE Publishing, London, 2011.
[21] S.E. Kichanov, M. Kenessarin, M. Balasou, D.P. Kozlenko, M. Nicu, L. Ionascu, A. C. Dragolici, F. Dragolici, K. Nazarov, B. Abdurahimov, Studies of the processes of hardening of cement materials for the storage of aluminum radioactive waste by neutron radiography, Phys. Part. Nucl. Lett. 17 (2020) 73–78.
[22] D.P. Kozlenko, S.E. Kichanov, E.V. Lukin, B.N. Savenko, The DN-6 Neutron diffractometer for high-pressure research at half a megabar scale, Crystals 8 (2018) 1–9.
[23] J. Rodriguez-Carvajal, Recent advances in magnetic structure determination by neutron diffraction, Physica B 192 (1993) 55–69.
[24] D.P. Kozlenko, S.E. Kichanov, E.V. Lukin, A.V. Rutkauskas, A.V. Belushkin, G. D. Bokuchava, B.N. Savenko, Neutron radiography and tomography facility at IBR-2 reactor, Phys. Part. Nucl. 13 (2016) 346–351.
[25] C.A. Schneider, W.S. Rasband, K.W. Eliceiri, NIH Image to ImageJ: 25 years of image analysis, Nat. Methods 9 (2012) 671–675.
[26] F. Brun, SYRMEP Tomo Project: a graphical user interface for customizing CT reconstruction workflows, Advanced Structural and Chemical Imaging 3 (2017) 1–9.
[27] J.W. Anthony, R.A. Bideaux, K.W. Bladh, M.C. Nichols, Handbook of Mineralogy, Mineral Data Publishing, Arizona, 1990.
[28] G.C. Bye, Portland Cement: Composition, Production and Properties, Thomas Telfrod Publishing, London, 1999.

[29] S.E. Kichanov, K.M. Nazarov, D.P. Kozlenko, M. Balasoiu, M. Nicu, L. Ionascu, A. C. Dragolici, F. Dragolici, B.N. Savenko, Neutron tomography studies of cement-based material used for radioactive waste conditioning, Romanian physics of journal 64 (2019) 803–812.
[30] G. van Dalen, M.W. Koster, 3D visualisation and quantification of bubbles in emulsions using μCT and image analysis. Proceedings of the 13th International Congress of Stereology (ICS-13), October, Beijing, China, 2011, pp. 19–23, https://doi.org/10.13140/2.1.4178.4643.
[31] P. Christe, M. Bernasconi, P. Vontobel, P. Turberg, A. Parriaux, Three-dimensional petrographical investigations on borehole rock samples: a comparison between X-ray computed- and neutron tomography, Acta Geotechnica 2 (4) (2007) 269–279, https://doi.org/10.1007/s11440-007-0045-9.
[32] W. Pabst, E. Gregorova, Characterization of Particles and Particle Systems, ICT, Prague, 2007.
[33] G. Henk, Particle Size Measurements, Springer, Netherlands, 2009.
[34] G.J. Dvorak, Micromechanics of Composite Materials, Springer, Netherlands, 2013.
[35] E.J. Routh, The Advanced Part of a Treatise on the Dynamics of a System of Rigid Bodies, McMilan, London, 1884.
[36] L.D. Landau, E.M. Lifshitz, Mechanics, third ed., Nauka, Moscow, 1993.
[37] H.-J. Bunge, Texture Analysis in Materials Science, London, first ed., Butterworth & Co, 1982.